Reduced linewidth multipolar plasmon resonances in metal nanorods and related applications†

Shunping Zhang,[ab] Li Chen,[ac] Yingzhou Huang[d] and Hongxing Xu[*abe]

Using dark-field scattering spectroscopy, we study the multipolar plasmon resonances in single crystallized silver nanorods. The lineshapes and homogenous linewidths of the surface plasmon resonances (SPRs) of different orders are analyzed and compared. The high-order resonances are found to sustain asymmetric Fano lineshapes and their linewidths are narrower than the dipolar resonance. A quantitative comparison using the finite element method reveals more than a three times reduction in the linewidth for the third order resonance, as compared with the dipolar one. These narrow linewidths result from the smaller radiative damping of the multipolar SPRs. Benefiting from the reduced damping, multipolar SPRs in nanorods are better candidates for many plasmonic applications, including increased-sensitivity single particle SPR sensors and reduced-threshold nanolasers.

Metallic nanoparticles (MNPs), supporting a group of collective motions of the conduction electrons, known as plasmons, are extensively investigated in nanophotonics due to their peculiar and tunable optical properties.[1] MNPs can function as effective optical antennas, with the capability of capturing electromagnetic radiation in their vicinity or transmitting the electromagnetic radiation from a nearby local emitter into the far-field.[2,3] The concentration of an electromagnetic field into a nanometer scale space, *e.g.* interparticle gaps between MNPs, produces an enormous electromagnetic field enhancement that can boost the excitation and emission rate of a local emitter.[4,5] Therefore, MNPs are ideal amplifiers for many weak optical processes, such as Raman scattering, fluorescence and harmonics generation, *etc.*[6-11] On the other hand, MNPs can be used as local chemical or biological probes due to the fact that the localized surface plasmon resonances (LSPRs) depend strongly on the dielectric environment around the MNPs.[12] In all the above mentioned and many other LSPR-based applications, the performance of the system is usually related to, or hampered by, a low quality factor Q, which is ultimately limited by the Ohmic loss that is inherently associated with the metal components.[13] For example, the local field enhancement that a very small MNP can provide is in the order of $\sim Q$.[14] By definition, the figure of merit (FoM) of LSPR sensing[15] is also proportional to Q. In realistic situations, besides Ohmic loss which is nonradiative, surface plasmons also suffer from radiative damping. For particles larger than 60 nm, radiative damping is considered to dominate over the Ohmic loss and significantly broaden the LSPR linewidths.[14] As the volume of a MNP increases, the number of conduction electrons involved in the collective motions increases so that the dipole moment of the surface plasmon is larger. The resonance is more radiatively damped, resulting in a poorer quality factor for big MNPs.[16] However, for multipolar LSPRs, the radiation strength is usually much weaker so that the modes are always 'dark'. With suppressed radiative damping, the linewidths and the quality factors of the multipolar LSPRs can, in principle, get close to the quasi-static limit. A good example showing the merit of dark modes is the Fano resonance arising from the interference of a superradiative and a subradiative mode. The local field enhancement near the Fano dip (position of the dark mode) is shown to be much higher than at other positions[17] while the FoM of LSPR sensing can be significantly improved.[18,19]

However, for MNPs of spherical or other similar shapes, the multipolar LSPRs of different orders are usually located very close to each other, making the extraction of their linewidths and lineshapes difficult. Compared with spherical MNPs, the LSPRs in metallic nanorods depend linearly on the aspect ratio of the nanorods and can be routinely tailored.[20-22] With an elongated dimension, a nanorod can sustain longitudinal surface plasmon modes that travel back and forth along the rod axis. Once the surface plasmon accumulates a $2n\pi$ ($n = 1, 2, 3, \ldots$) phase shift from the round trip between the two facets (like mirrors), it becomes resonant. Therefore, these multipolar plasmon resonances in a nanorod can be well described by a

[a]Beijing National Laboratory for Condensed Matter Physics and Institute of Physics, Chinese Academy of Sciences, Box 603-146, Beijing 100190, China. E-mail: hxxu@iphy.ac.cn

[b]Center for Nanoscience and Nanotechnology, School of Physics and Technology, Wuhan University, Wuhan 430072, China

[c]Department of Applied Physics, Hunan University, Changsha 410082, China

[d]Department of Applied Physics, Chongqing University, Chongqing 400044, China

[e]Division of Solid State Physics/The Nanometer Structure Consortium, Lund University, Box 118, S-22100, Lund, Sweden
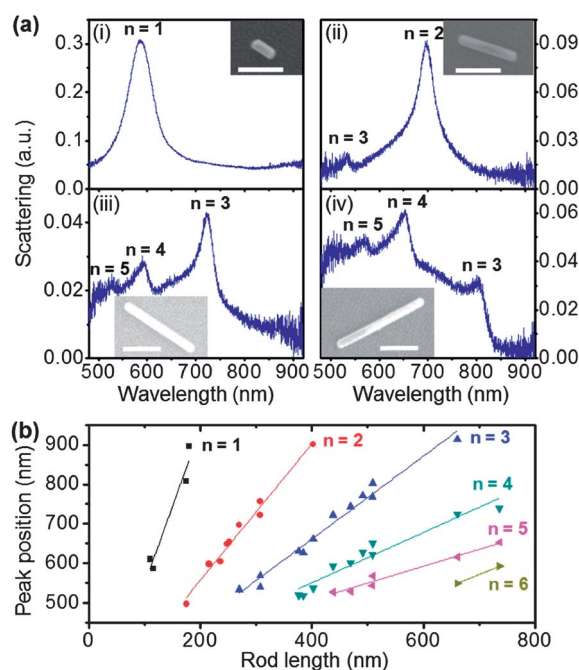
† Electronic supplementary information (ESI) available. See DOI: 10.1039/c3nr01219k

damped Fabry–Pérot model and are well separated in the spectral domain.[23–25] Such a feature enables metal nanorods to be ideal platforms for a multipolar LSPR study. The spatial extension of multipolar plasmon resonances in nanorods has been imaged directly by several groups using, e.g. cathodoluminescence spectroscopy,[26] scanning near-field optical microscopy[25] and most recently by electron microscopy with unprecedented resolution.[27–29] The high spatial resolution enables the observation of surface plasmon antinode bunching at the nanorod terminals.[27] However, as a trade-off, the energy resolution in electron energy loss spectroscopy (EELS) is usually limited, e.g., to 100 meV in ref. 27 or 450–500 meV in ref. 28. Therefore, it is difficult to extract the narrow linewidths of multipolar plasmon resonances by EELS. Optical measurements on the other hand provide a much better energy resolution. However, previous optical spectroscopy studies on the multipolar LSPRs of metal nanorods were usually carried out on assemblies of nanorods, like a planar array or in solution.[30–33] These studies suffer from inhomogeneous broadening. The choice of substrate may cause additional broadening in previous dark-field measurements on individual rice-shaped silver nanoparticles.[34] Although theoretical calculations have clearly shown the reduced linewidth and a significant improvement in the quality factor for the second order plasmon resonances in rod-shaped MNPs,[35] experimental observations have not yet been reported. Recent calculations have also shown that an asymmetric Fano lineshape may appear in the scattering spectrum of a single rod-shaped MNP, originating from the interference between the adjacent odd-order modes.[36,37] In this article, we present a combined experimental and theoretical study on the lineshapes and homogeneous linewidths of the multipolar plasmon resonances of individual silver nanorods using dark-field scattering spectroscopy. We show that at the same energy position, the linewidths of the multipolar plasmon modes in a longer nanorod are narrower than the linewidths of the dipolar mode in a shorter nanorod. Asymmetric lineshapes in the high-order multipolar plasmon modes are observed. Though it is well understood conceptually, to the best of our knowledge, we are the first to provide quantitative experimental confirmation that multipolar LSPRs possess lower losses and higher quality factors, compared to the dipolar ones. Benefitting from the reduced radiative damping, the use of multipolar plasmon resonances leads to a four-fold increase in the FoM of LSPR sensing and a four-time reduction in the threshold of a gain compensation nanolaser.

Crystalline Ag nanorods were synthesized using a sol–gel method.[38] 150 mg of poly(vinyl pyrrolidone) (PVP, K130) and 0.6 ml of 1 M $AgNO_3$ aqueous solution were added to a 12 ml ethylene glycol (EG) solution. After stirring for half an hour, the whole solution was added drop by drop into 5 ml of EG at 160 °C. After the $AgNO_3$ was completely reduced (~60 min), the solution was cooled, washed via centrifugation once in acetone to remove the EG, then twice in ethanol to remove the PVP. The diameters of the nanorods are typically around 28–36 nm, while the lengths range from tens of nanometers to several micrometers. The nanorods, dispersed in ethanol, were simply dripped onto a cleaned glass slice and allowed to dry. After that, an indexed copper grid was attached to the sample, which enabled the correlation of the measured optical spectra and morphology characterization using scanning electron microscopy (SEM). Scattering spectra of individual Ag nanorods were taken by a transmission type dark-field microscope coupled to a confocal Raman spectrometer (Renishaw, Invia). Non-polarized white light from a halogen lamp was incident from the bottom, scattered by the nanorod, collected by a 100× objective (N.A. = 0.85) and then directed to an air-cooled CCD after passing through the grating (1800 lines per mm). A background spectrum taken from a nearby area of a bare glass surface was subtracted from each measured nanorod spectrum. After the optical measurements, a thin Au layer (about 6 nm) was deposited onto the sample to ensure the conductivity required by the SEM. This made the nanorods appear thicker in the SEM images than their actual sizes.

Typical scattering spectra of Ag nanorods (diameter restricted to around 35 nm) of different lengths are shown in Fig. 1(a) and the corresponding SEM images are shown in the insets. The resonant orders ($n = 1–5$) are indicated on top of each peak. For the short nanorod (i), length $L = 104$ nm, only the dipolar peak ($n = 1$) appears. As the length increases (ii), $L = 258$ nm, high order ($n = 2, 3$) modes can be observed while the dipolar mode is red-shifted outside the range of our measurements. As the length of the nanorod is further increased to $L = 426$ nm (iii) or 497 nm (iv), higher order modes ($n = 4, 5$) appear, while the second order mode is red-shifted out of range. The relatively low peak intensity of the $n = 3$ mode in (iv) may be due

Fig. 1 (a) Dark-field scattering spectra of Ag nanorods (diameter $D \sim 35$ nm) of different lengths, $L = 104$ nm (i), 258 nm (ii), 426 nm (iii) and 497 nm (iv). The resonant orders are denoted on top of each peak and the SEM images of the corresponding nanorods are shown in the insets. The scale bars are 200 nm. (b) Resonant peak positions as a function of the length of the nanorods. The diameters of the rods are restricted to a small range of 35 ± 3 nm, determined by SEM.

to a reduced collection efficiency in our setup in the longer wavelength region for long nanorods (see ESI†). For longer nanorods ($L > 800$ nm), the excitation efficiency for the multipolar plasmon resonances by a plane wave becomes smaller so that the obtained scattering peaks are undistinguishable (see Fig. S4†). Fig. 1(b) summarizes the resonant peak positions as a function of the nanorod length. Clearly, modes of different orders fall into different regions in such a way that the peak positions depend linearly on the nanorod length for each resonant order. Linear fits yield the dependence of resonant wavelength λ_n and the nanorod length, e.g., $\lambda_1 = 3.94L + 152$ for the dipolar mode and $\lambda_2 = 1.73L + 211$ for the second order mode. The results of the fits are listed in Table 1. As the resonant order increases, the fitted slope decreases, and the intercept increases, in agreement with theoretical predictions.[7,39]

Recent calculations show that the lineshapes of the multipolar plasmon resonances in a rod-shaped MNP exhibit asymmetric Fano profiles.[36,37] As a coherent process, the Fano interference takes place between two modes (more strictly, two paths) that can partly overlap in both the spatial and energy domains. For plasmonic nanoparticles, the Fano interference usually involves a bright and a dark mode that are not far apart. Specifically, for a nanorod, the asymmetric Fano lineshape is pronounced for the $n = 3$ mode, originating from the interference with the tail of the bright dipolar mode.[37] To extract the shape function and the linewidth of the resonant peaks, the scattering spectra are fitted by the following Fano lineshape (more terms were added according to the number of peaks)
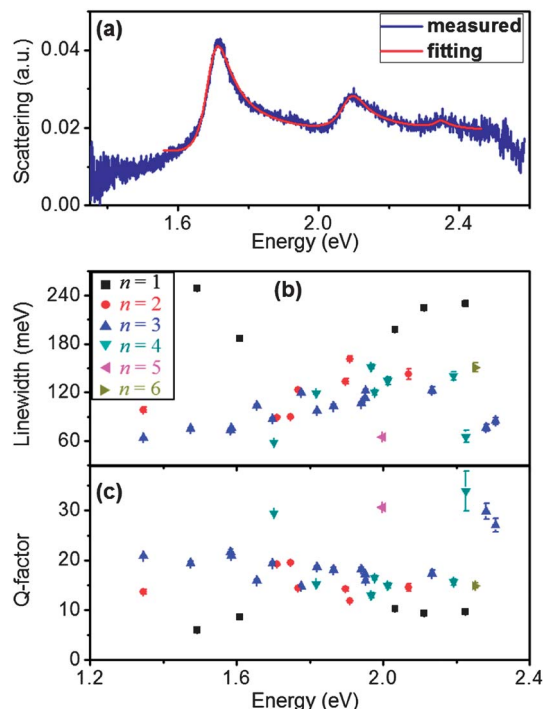
$$y = B + A\left(q + \frac{\omega - \omega_n}{\Gamma/2}\right)^2 / \left[1 + \left(\frac{\omega - \omega_n}{\Gamma/2}\right)^2\right], \quad (1)$$

where A and B are the fitting coefficients, ω_0 and Γ are the resonant energy and the full width of the SPRs. The Fano factor q describes the degree of asymmetry of the peak. Fig. 2(a) shows that for the nanorod shown in Fig. 1(a)iii, the scattering peaks ($n = 3, 4, 5$) exhibit clear asymmetric lineshapes. The Fano fitting reproduces the asymmetric profiles of the resonant peaks nicely, yielding $\Gamma = 87.6$ meV (92.5 meV) and $q = 2.66$ (3.75) for $n = 3$ (4). Note that the fitting results for the $n = 5$ resonance fluctuate with the fitting range. We varied the fitting range until a maximized fitting R-square parameter was achieved. Few of the measured peaks, like the $n = 3$ mode in the (iv) panel of Fig. 1(a), were not well fitted by eqn (1) and were excluded in the analysis in the following. Though different from rod to rod,

Fig. 2 (a) Scattering spectrum of the same nanorod as shown in Fig. 1(a)iii. The red line is the Fano fit. (b and c) Linewidths (b) and quality factors (c) of nanorod LSPRs of different orders: $n = 1$ (black squares), 2 (red dots), 3 (blue up triangles), 4 (green down triangles), 5 (magenta left triangles) and 6 (khaki right triangles). The diameters of the rod are restricted to 35 ± 5 nm. The error bars in (b) and (c) are taken from the standard deviations of the fits.

typical values for the asymmetric factor q are around 2.5 and 3.5 for $n = 3$ and 4, which are much smaller than those for $n = 1$ and 2 (see Fig. S5†). Fig. 2(b) shows the fitted linewidths of the measured nanorods (diameter 35 ± 5 nm) of different lengths. Despite the fluctuation among different nanorods, the linewidths of multipolar ($n \geq 2$) LSPRs are narrower than those of the dipolar mode. Typically, Γ is 180–250 meV for the dipolar mode, 80–170 meV for $n = 2$ and 60–130 meV for $n = 3$. The quality factor can be deduced from the linewidth by $Q = \omega_n/\Gamma$. As shown in Fig. 2(c), multipolar plasmon resonances sustain a higher quality factor than the dipolar mode, i.e., Q is less than or around 10 for $n = 1$, but increases to around and larger than 15 for $n = 2$ and 3. The highest quality factor obtained in the experiments exceeds 30. In a system without gains, the material loss places an upper limit for the quality factor of LSPRs in the quasi-static limit, determined by $Q = \omega(d\varepsilon'_m/d\omega)(2\varepsilon''_m)^{-1}$, where ε'_m and ε''_m are the real and imaginary parts of the permittivity of the metal.[13] As revealed here, multipolar plasmon resonances sustain a better quality factor approaching this limit. We note that the measured linewidths and quality factors vary from rod to rod. This is most probably due to the difference in the diameter, geometry of the terminals and the exact dielectric environment around the nanorods.
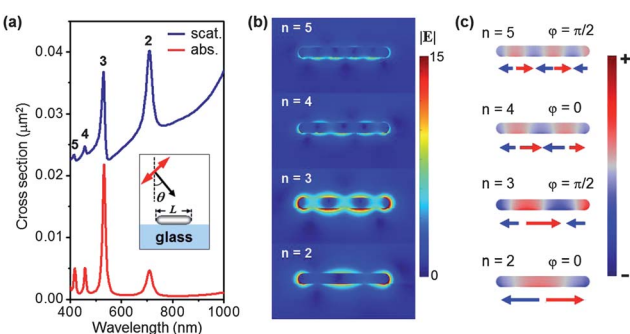
To compare more quantitatively the LSPRs of different orders in a single metallic nanorod, we performed numerical calculations using a commercial finite element method (FEM) package (COMSOL Multiphysics). Instead of using an effective

Table 1 Results of the linear fits ($\lambda_n = aL + b$) in Fig. 1(b)[a]

Resonant order	Slope, a	Intercept, b (nm)	R^2-factor
$n = 1$	3.94 ± 0.66	152 ± 98	0.9209
$n = 2$	1.730 ± 0.087	211 ± 24	0.9804
$n = 3$	1.052 ± 0.048	240 ± 21	0.9781
$n = 4$	0.639 ± 0.058	295 ± 30	0.9309
$n = 5$	0.429 ± 0.037	334 ± 21	0.9647

[a] The standard deviations for $n = 1$ are large because there are only four points. Those for $n = 6$ are not included since there are only two points available.

homogenous medium as the background, the effect of the substrate was fully taken into account by the simulation model using the Fresnel formulae as background fields.[19] The nanorod, with a circular cross-section, was laid directly on the glass substrate (refractive index, $n_s = 1.5$). The permittivity of Ag was taken from the experimental data reported by Johnson and Christy.[40] The terminals of the nanorod were simply modeled as hemispheres, which were included in the definition of the length of the nanorod, see the inset in Fig. 3(a). An oblique incident p-polarized plane wave, with an angle θ to the substrate normal, was used as the excitation. Fig. 3(a) shows the scattering and absorption cross-section of a 300 nm long Ag nanorod deposited on glass. As in the experiment, multipolar plasmon resonances of neighboring order are accessible for oblique incidence. The scattering spectrum shows a clear asymmetric lineshape at the $n = 3$ resonance, while the absorption peaks remain Lorentzian. Fig. 3(b) shows the near-field distribution at each absorption peak shown in Fig. 3(a). As previously mentioned, the multipolar plasmon resonances can be viewed as Fabry–Pérot cavity modes that travel along the nanorod axis and get reflected at the terminals. When the round trip travel accumulates a $2n\pi$ phase shift, it becomes resonant so that the electromagnetic energy is trapped around the nanorod. In this standing wave picture, the nth-order mode has n nodes along the nanorod axis, as shown in Fig. 3(b). Using this Fabry–Pérot model, the multipolar plasmon resonances fall in to a "dispersion relationship" that agrees well with the fundamental surface plasmon polariton (SPP) mode, called the H_0 mode, on an infinitely long nanowire over a dielectric substrate system.[41] Fig. 3(b) also shows that the near-field enhancement is stronger for the 3rd-order mode compared with the other modes ($n = 2, 4$ and 5). This is mainly due to the efficient excitation of this mode under near normal incident ($\theta = 15°$), as judged from the radiation pattern of this mode.[24]

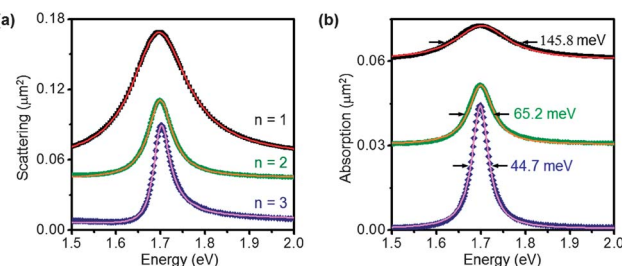The calculated scattering and absorption spectra show sharp resonances for the resonant orders $n \geq 2$, in agreement with the experimental results. Fig. 3(c) shows the surface charge distributions corresponding to each multipolar resonance. The instantaneous phase φ comes from the factor $e^{i\varphi} = e^{-i\omega t}$ for a time harmonic field. Similar to the local excitation of a nanowire SPP mode at the terminal,[42] the excitation of plasmon modes with different spatial extensions may be interpreted to "happen" at a distinct phase delay. The $n = 3$ and 5 resonances are maximally "excited" at $\varphi = \pi/2$ compared with $\varphi = 0$ for $n = 2$ and 4. Fig. 3(c) also explains the narrow linewidths of the multipolar plasmon resonances in the nanorod. Unlike the dipolar mode, all the surface charges are distributed in such a way that all the modes possess a small net dipole moment. If the system is scaled down to the quasi-static limit, these kinds of charge distributions are inaccessible by light and are totally dark. However, the finite size of the nanorod, particularly its length L in the order of excitation wavelength, guarantees that the retardation effect is significant and the multipolar plasmon resonances are therefore accessible by light. For the current size of the nanorods in this study, the coupling strengths to light are still weak so that the radiative damping is small. Another equivalent understanding of the reduced linewidth for the multipolar plasmon resonances can be modeled within the damped Fabry–Pérot model. The internal Ohmic loss inside the metal is replaced by propagation decay along the cavity, while the radiative loss is modeled by the transmission loss at the end-facet mirror. Since the surface plasmon experiences reflection twice for each round trip, the decay constant via the end-facet mirror is $-\ln (R)/L$, where R is the reflectivity of the mirror.[43] This value is typically larger than the attenuation constant of the SPP for the current size and energy range of the nanorod. Therefore, longer nanorods suffer less reflection loss and have sharper resonant peaks.

A quantitative comparison of the lineshapes and linewidths of the $n = 1$–3 order LSPRs in a single Ag nanorod is shown in Fig. 4. By varying the length of the nanorod, the LSPRs of different orders are tuned to the same energy position, $\lambda_n = 730$ nm ($\omega_n = 1.698$ eV). As mentioned above, the scattering peak for the $n = 3$ order resonance exhibits a clear asymmetric Fano lineshape. A fit using eqn (1) yields an asymmetric Fano factor $q = 6.356$. The presence of a dielectric substrate can mediate the coupling of different LSPRs in a nearby MNP and lead to Fano resonances.[19,44] However, the Fano interference presented here

Fig. 3 (a) FEM calculated scattering (blue) and absorption (red) cross-section of a Ag nanorod ($D = 35$ nm, $L = 300$ nm) supported on a glass substrate. The resonance orders $n = 2$–5 are indicated on the top of each peak. Electric field $|E|$ (b) and surface charge (c) distribution at the resonant peaks: $\lambda_n = 418$ nm ($n = 5$), 457 nm ($n = 4$), 532 nm ($n = 3$) and 708 nm ($n = 2$). The red and blue arrows schematically show that the total dipole momentum along the nanorod is zero. The φ in (c) represents the instantaneous phase at which the surface charge is plotted. As indicated in the inset in (a), the nanorod is excited by a p-polarized plane wave with an incident angle $\theta = 15°$.

Fig. 4 FEM calculated scattering (a) and absorption (b) cross-sections of a single Ag nanorod ($D = 35$ nm) supported on a glass substrate. The length of the nanorod $L = 142.4$ nm (black squares), 311.6 nm (green dots) and 482.3 nm (blue diamonds). The incident angle $\theta = 0°$ for $n = 1, 3$, and $\theta = 45°$ for $n = 2$. The lines are Fano (a) and Lorentz (b) fits to the calculated points. For clarity, the curves for $n = 1, 2$ are shifted vertically.
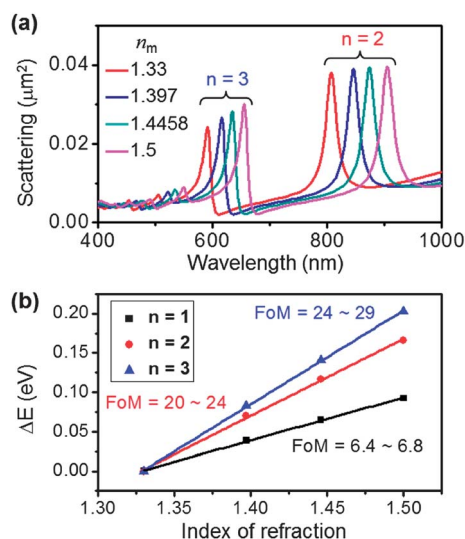
is attributed to the interference between adjacent odd (or even) nanorod modes,[37] which is also pronounced in the absence of a substrate. As shown in Fig. 4(b), fitting the absorption peaks using the Lorentzian function yields the linewidth $\Gamma = 145.8$ meV, 65.2 meV and 44.7 meV for $n = 1$, 2 and 3, respectively. Usually, for a MNP of given shape, the LSPR linewidths become broader for a larger particle size due to the stronger radiative damping.[14,16] However, Fig. 4 reveals the opposite behavior. The linewidth of the $n = 3$ mode on the 482.3 nm long nanorod is only 30.7% of that of the dipolar mode on the 142.4 nm long nanorod. In terms of quality factor, the resonance is improved from $Q = 11.67$ for the dipolar mode to 26.08 and 37.99 for the 2nd and 3rd order resonances. Of cause, the present conclusion is not to overturn the general statement that larger MNPs have stronger radiative damping, but to emphasize that it is valid only when comparing the modes of the same order.
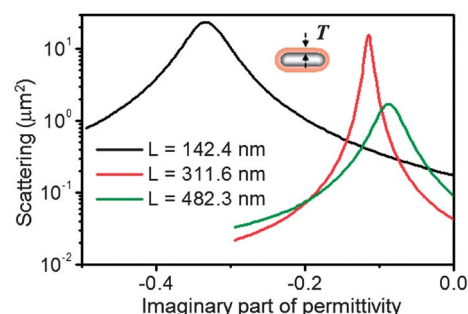
The reduced linewidths of the multipolar plasmon resonances are of critical importance in many LSPR-based applications. In the following, we will show two examples, namely, the LSPR sensing, and loss compensation by gain materials. For simplicity, the glass substrate is not included in the following, aiming to simulate nanorods suspended in a solution. Fig. 5(a) shows the scattering cross-section for a single nanorod embedded in different matrices with refractive indices n_m, corresponding to some commonly used liquids.[18] As expected, the LSPR red-shifts as n_m increases. As shown in Fig. 5(b), linear regressions yield the sensitivity, namely, the energy shift per refractive index unit (RIU), of 0.5433 eV per RIU, 0.9764 eV per RIU and 1.192 eV per RIU for the $n = 1$–3 resonances. Defined as the ratio of sensitivity to the full linewidth of the peaks, the FoM provides a fairly good characterization for comparing different LSPR sensors.[15] Benefiting from the narrower linewidths, the FoM for multipolar LSPR sensing can be improved by about a

factor of four, *i.e.* FoM = 24–29 for $n = 3$ compared to 6.4–6.8 for $n = 1$. Therefore, longer nanorods are better LSPR sensors, as proposed in a recent study where the Fano interference but not the linewidth was emphasized.[45]

Another attractive LSPR-based application is to design nanolasers,[43,46] based on surface plasmon amplification by simulated emission of radiation (SPASER).[47] However, the lossy characteristic associated with LSPRs imposes a high gain threshold for lasing. Dipolar plasmon resonances in metallic nanorods were shown to have a dramatically reduced damping compared with those in spherical nanoparticles.[48] This smaller damping converts to nearly a one order reduction in the threshold of nanorod-based SPASERs.[49] Although a strict calculation of gain compensation in nanostructures is rather complicated, we have adapted a simple approach by adding a negative imaginary part to the permittivity of the gain material. This model assumes an unrealistic, uniform spatial distribution of gain but otherwise provides a qualitative estimation of the gain coefficients required by the system. To avoid the extension of the electromagnetic field into the perfectly matched layers in FEM simulations near the threshold of loss compensation, the calculations were carried out using the boundary element method (BEM). Since only the scatters need to be discretized, BEM can provide a fairly good calculation of the amplified scattering or absorption cross-sections. The gain material is modeled by a 20 nm thick dielectric shell (permittivity $\varepsilon_{gain} = 2.25 - i\varepsilon''_{gain}$), coated uniformly onto the nanorods presented in Fig. 4. The surrounding medium was chosen to be water in view of most experimental realizations.[46] Due to the screening effect, the LSPRs are red-shifted to 913 nm, 884 nm and 874 nm for $n = 1$, 2 and 3, respectively. Fig. 6 shows the scattering cross-sections of a coated nanorod at each resonant position, as a function of the imaginary part of the permittivity of the coating material. The LSPRs reach their lasing thresholds at $\varepsilon''_{gain} = 0.335$, 0.115 and 0.085 for $n = 1$, 2 and 3. As expected, the multipolar LSPRs need much smaller gain coefficients to fully compensate their loss. Comparing the $n = 1$ and $n = 3$ modes, about a four-time reduction in gain threshold is obtained. Therefore, multipolar LSPRs in metallic

Fig. 5 (a) FEM calculated scattering cross-sections of a single Ag nanorod ($D = 35$ nm, $L = 300$ nm) embedded in different matrices with refractive indices $n_m =$ 1.33 (water, red), 1.397 (butanol, blue), 1.4458 (chloroform, green) and 1.5 (oil, magenta). The incident angle is $\theta = 15°$. (b) Linear plot of LSPR shifts of $n = 1$–3 order modes as a function of refractive index n_m.

Fig. 6 BEM calculated scattering cross-section of a Ag nanorod ($D = 35$ nm) of different lengths, $L = 142.4$ nm (black), 311.6 nm (red) and 482.3 nm (green), as a function of the imaginary part of the permittivity of the coating gain material. The calculations were taken at resonant positions of the LSPRs, $\lambda_n = 913$ nm, 884 nm and 874 nm for $n = 1$–3. The real part of the permittivity of the coating layer (thickness $T = 20$ nm) is 2.25. The coated nanorod is embedded in water.

nanorods are a more realistic test-bed for achieving single nanoparticle SPASERs.

In conclusion, we have performed dark-field scattering measurements on individual Ag nanorods. Correlated optical and morphology studies enable us to investigate the dependence of the LSPR position and the nanorod length. We investigate the lineshapes and linewidths of the LSPRs of different orders and find that multipolar LSPRs exhibit asymmetric Fano lineshapes and their linewidths are significantly smaller than the dipolar mode. The weak ability to radiate, *i.e.*, a smaller radiative damping, is the main reason for the narrow linewidths. Multipolar LSPRs have an increase in quality factor approaching the quasi-static limit. Electromagnetic simulations based on FEM show the scattering and absorption cross-sections, local field enhancement and surface charge distribution of a substrate-supported nanorod. Quantitative comparison between modes of different order is performed by FEM, which supports the experimental observations. We further propose to use these nanorod multipolar plasmon resonances for increased-sensitivity LSPR sensors and reduced-threshold SPASERs. A four-fold increase in the FoM of LSPR sensing and a four-time reduction in the threshold of gain compensation nanolasers are predicted.

Acknowledgements

References

1 N. J. Halas, S. Lal, W. S. Chang, S. Link and P. Nordlander, *Chem. Rev.*, 2011, **111**, 3913–3961.

2 L. Novotny and N. van Hulst, *Nat. Photonics*, 2011, **5**, 83–90.

3 P. Biagioni, J. S. Huang and B. Hecht, *Rep. Prog. Phys.*, 2012, **75**, 024402.

4 H. X. Xu, J. Aizpurua, M. Käll and P. Apell, *Phys. Rev. E: Stat. Phys., Plasmas, Fluids, Relat. Interdiscip. Top.*, 2000, **62**, 4318–4324.

5 H. X. Xu, X. H. Wang, M. P. Persson, H. Q. Xu, M. Käll and P. Johansson, *Phys. Rev. Lett.*, 2004, **93**, 243002.

6 M. Moskovits, *Rev. Mod. Phys.*, 1985, **57**, 783–826.

7 J. Aizpurua, G. W. Bryant, L. J. Richter, F. J. G. de Abajo, B. K. Kelley and T. Mallouk, *Phys. Rev. B: Condens. Matter Mater. Phys.*, 2005, **71**, 235420.

8 O. L. Muskens, V. Giannini, J. A. Sánchez-Gil and J. G. Rivas, *Nano Lett.*, 2007, **7**, 2871–2875.

9 P. Mühlschlegel, H. J. Eisler, O. J. F. Martin, B. Hecht and D. W. Pohl, *Science*, 2005, **308**, 1607–1609.

10 S. Kim, J. H. Jin, Y. J. Kim, I. Y. Park, Y. Kim and S. W. Kim, *Nature*, 2008, **453**, 757–760.

11 M. Agio, *Nanoscale*, 2012, **4**, 692–706.

12 K. M. Mayer and J. H. Hafner, *Chem. Rev.*, 2011, **111**, 3828–3857.

13 F. Wang and Y. R. Shen, *Phys. Rev. Lett.*, 2006, **97**, 206806.

14 M. I. Stockman, *Opt. Express*, 2011, **19**, 22029–22106.

15 L. J. Sherry, S. H. Chang, G. C. Schatz, R. P. Van Duyne, B. J. Wiley and Y. N. Xia, *Nano Lett.*, 2005, **5**, 2034–2038.

16 M. Hu, C. Novo, A. Funston, H. N. Wang, H. Staleva, S. L. Zou, P. Mulvaney, Y. N. Xia and G. V. Hartland, *J. Mater. Chem.*, 2008, **18**, 1949–1960.

17 J. Ye, F. F. Wen, H. Sobhani, J. B. Lassiter, P. Van Dorpe, P. Nordlander and N. J. Halas, *Nano Lett.*, 2012, **12**, 1660–1667.

18 J. B. Lassiter, H. Sobhani, J. A. Fan, J. Kundu, F. Capasso, P. Nordlander and N. J. Halas, *Nano Lett.*, 2010, **10**, 3184–3189.

19 S. P. Zhang, K. Bao, N. J. Halas, H. X. Xu and P. Nordlander, *Nano Lett.*, 2011, **11**, 1657–1663.

20 S. Link, M. B. Mohamed and M. A. El-Sayed, *J. Phys. Chem. B*, 1999, **103**, 3073–3077.

21 G. W. Bryant, F. J. G. De Abajo and J. Aizpurua, *Nano Lett.*, 2008, **8**, 631–636.

22 H. Chen, L. Shao, Q. Li and J. Wang, *Chem. Soc. Rev.*, 2012, **42**, 2679–2724.

23 J. Dorfmüller, R. Vogelgesang, R. T. Weitz, C. Rockstuhl, C. Etrich, T. Pertsch, F. Lederer and K. Kern, *Nano Lett.*, 2009, **9**, 2372–2377.

24 T. H. Taminiau, F. D. Stefani and N. F. van Hulst, *Nano Lett.*, 2011, **11**, 1020–1024.

25 E. Cubukcu and F. Capasso, *Appl. Phys. Lett.*, 2009, **95**, 201101.

26 E. J. R. Vesseur, R. de Waele, M. Kuttge and A. Polman, *Nano Lett.*, 2007, **7**, 2843–2846.

27 D. Rossouw, M. Couillard, J. Vickery, E. Kumacheva and G. A. Botton, *Nano Lett.*, 2011, **11**, 1499–1504.

28 B. S. Guiton, V. Iberi, S. Z. Li, D. N. Leonard, C. M. Parish, P. G. Kotula, M. Varela, G. C. Schatz, S. J. Pennycook and J. P. Camden, *Nano Lett.*, 2011, **11**, 3482–3488.

29 H. Liang, H. Zhao, D. Rossouw, W. Wang, H. Xu, G. A. Botton and D. Ma, *Chem. Mater.*, 2012, **24**, 2339–2346.

30 J. R. Krenn, G. Schider, W. Rechberger, B. Lamprecht, A. Leitner, F. R. Aussenegg and J. C. Weeber, *Appl. Phys. Lett.*, 2000, **77**, 3379–3381.

31 E. K. Payne, K. L. Shuford, S. Park, G. C. Schatz and C. A. Mirkin, *J. Phys. Chem. B*, 2006, **110**, 2150–2154.

32 H. M. Bok, K. L. Shuford, S. Kim, S. K. Kim and S. Park, *Nano Lett.*, 2008, **8**, 2265–2270.

33 V. Giannini, G. Vecchi and J. G. Rivas, *Phys. Rev. Lett.*, 2010, **105**, 266801.

34 H. Wei, A. Reyes-Coronado, P. Nordlander, J. Aizpurua and H. X. Xu, *ACS Nano*, 2010, **4**, 2649–2654.

35 G. Della Valle, T. Søndergaard and S. I. Bozhevolnyi, *Opt. Express*, 2008, **16**, 6867–6876.

36 J. M. Reed, H. N. Wang, W. F. Hu and S. L. Zou, *Opt. Lett.*, 2011, **36**, 4386–4388.

37 F. López-Tejeira, R. Paniagua-Domínguez, R. Rodríguez-Oliveros and J. A. Sánchez-Gil, *New J. Phys.*, 2012, **14**, 023035.

38 C. Damm, D. Segets, G. A. Yang, B. F. Vieweg, E. Spiecker and W. Peukert, *Small*, 2011, **7**, 147–156.

39 L. Novotny, *Phys. Rev. Lett.*, 2007, **98**, 266802.

40 P. B. Johnson and R. W. Christy, *Phys. Rev. B: Solid State*, 1972, **6**, 4370–4379.

41 S. P. Zhang and H. X. Xu, *ACS Nano*, 2012, **6**, 8128–8135.

42 S. P. Zhang, H. Wei, K. Bao, U. Håkanson, N. J. Halas, P. Nordlander and H. X. Xu, *Phys. Rev. Lett.*, 2011, **107**, 096801.

43 R. F. Oulton, V. J. Sorger, T. Zentgraf, R. M. Ma, C. Gladden, L. Dai, G. Bartal and X. Zhang, *Nature*, 2009, **461**, 629–632.

44 H. J. Chen, L. Shao, T. Ming, K. C. Woo, Y. C. Man, J. F. Wang and H. Q. Lin, *ACS Nano*, 2011, **5**, 6754–6763.

45 F. López-Tejeira, R. Paniagua-Domínguez and J. A. Sánchez-Gil, *ACS Nano*, 2012, **6**, 8989–8996.

46 M. A. Noginov, G. Zhu, A. M. Belgrave, R. Bakker, V. M. Shalaev, E. E. Narimanov, S. Stout, E. Herz, T. Suteewong and U. Wiesner, *Nature*, 2009, **460**, 1110–1112.

47 D. J. Bergman and M. I. Stockman, *Phys. Rev. Lett.*, 2003, **90**, 027402.

48 C. Sönnichsen, T. Franzl, T. Wilk, G. von Plessen, J. Feldmann, O. Wilson and P. Mulvaney, *Phys. Rev. Lett.*, 2002, **88**, 077402.

49 S. Y. Liu, J. F. Li, F. Zhou, L. Gan and Z. Y. Li, *Opt. Lett.*, 2011, **36**, 1296–1298.